

Article

# The Impact of Pulse Charging Parameters on the Life Cycle of Lithium-Ion Polymer Batteries

J. M. Amanor-Boadu <sup>1,\*</sup>, A. Guiseppi-Elie <sup>2</sup>  and E. Sánchez-Sinencio <sup>1</sup>

<sup>1</sup> Department of Electrical and Computer Engineering, Texas A&M University, College Station, Texas 77840, USA; sanchez@ece.tamu.edu

<sup>2</sup> EnMed Working Group and Department of Biomedical Engineering, Texas A&M University, College Station, Texas 77840, USA; guiseppi@tamu.edu

\* Correspondence: judyboadu@tamu.edu; Tel.: +01-979-845-9583

Received: 2 August 2018; Accepted: 15 August 2018; Published: 18 August 2018



**Abstract:** The pulse charging algorithm is seen as a promising battery charging technique to satisfy the needs of electronic device consumers to have fast charging and increased battery charge and energy efficiencies. However, to get the benefits of pulse charging, the pulse charge current parameters have to be chosen carefully to ensure optimal battery performance and also extend the life cycle of the battery. The impact of pulse charge current factors on the life cycle and battery characteristics are seldom investigated. This paper seeks to evaluate the impact of pulse charge current factors, such as frequency and duty cycle, on the life cycle and impedance parameters of lithium-ion polymer batteries (LiPo) while using a design of experiments approach, Taguchi orthogonal arrays. The results are compared with the benchmark constant current-constant voltage (CC-CV) charging algorithm and it is observed that by using a pulse charger at optimal parameters, the cycle life of a LiPo battery can be increased by as much as 100 cycles. It is also determined that the duty cycle of the pulse charge current has the most impact on the cycle life of the battery. The battery impedance characteristics were also examined by using non-destructive techniques, such as electrochemical impedance spectroscopy, and it was determined that the ambient temperature at which the battery was charged had the most effect on the battery impedance parameters.

**Keywords:** Li-ion polymer battery; pulse charging; constant current constant voltage; electrochemical impedance spectroscopy; battery impedance; life cycle; Taguchi orthogonal arrays; design of experiments

## 1. Introduction

Lithium-ion (Li-ion) batteries have continued to increase their market share in the rechargeable battery market over the past few years [1,2]. They are projected to overtake the lead-acid battery market share by 2024 [3]. This is primarily driven by their superior qualities of high energy density, low self-discharge, and lack of memory effect [4]. They can be found in numerous devices and applications, ranging from electric vehicles to the Internet of Things (IoT) devices. Lithium-ion polymer (LiPo) batteries are analogous to their Li-ion counterparts, except for the use of a gel-like, polymer electrolyte, which serves to improve ion mobility [5]. They are commonly packaged in a pouch format that allows for the LiPo battery to be molded into many conformable form factors. LiPo batteries have the consumer-held, market-driven advantages of being lightweight and having good mechanical strength [4].

Fast charging, increased battery runtime, and increased battery charge and energy efficiencies are important characteristics that consumers of portable electronic applications desire. Though battery runtime can be improved by using various hardware and software techniques [6–8], these desirable

characteristics are impacted by the type of charging algorithm used, and as such, many charging algorithms have been proposed to achieve desirable and optimal output performance metrics. Of these charging algorithms, pulse charging is the most propitious [9–13]. Pulse charging is the application of carefully controlled charge current pulses into the battery. Figure 1 schematically illustrates the typical LiPo battery undergoing a charging process and shows the movement of the lithium ions ( $\text{Li}^+$ ), as they move from the positive electrode, cathode, through the separator to intercalate in the negative electrode, anode. During charging,  $\text{Li}^+$  arriving at the anode desolvate and diffuse within to become intercalated into the anode material. Issues that are related to desolvation dynamics, space-charge layers, and diffusion within the anode material may produce inefficiencies in the intercalation and result in accumulation of Li at the anode-electrolyte interface. If this is not abated, deposits grow into dendrite like structures [14] with the potential to penetrate the separator, leading to a thermal runaway [15]. To prevent this problem, the constant current-constant voltage (CC-CV) charging algorithm, which is considered as the benchmark charging algorithm, is used in many LiPo battery powered devices [16]. The CC-CV charging algorithm is shown in Figure 2. There are two major charging phases: constant current (CC) charge phase and the constant voltage (CV) charge phase. In the CC charge phase, a constant charge current ( $I_{\text{CHARGE}}$ ) is used to initially charge the battery. The battery voltage quickly rises in this region, as the  $\text{Li}^+$  can freely intercalate in the anode. When the voltage is approaching full charge ( $V_{\text{full}}$ ), the CC charge phase transitions to the CV charge phase, where the result is a decreasing charge current that prevents damage to the battery, ensures safety of the user, and allows time for the  $\text{Li}^+$  to properly intercalate. However, this CV region prolongs charge time due to the decreasing charge current used. Pulse charging does not have this drawback.

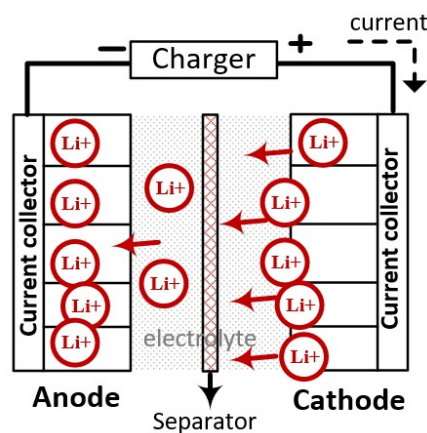


Figure 1. Schematic illustration of the charging process in a lithium-ion polymer (LiPo) battery.

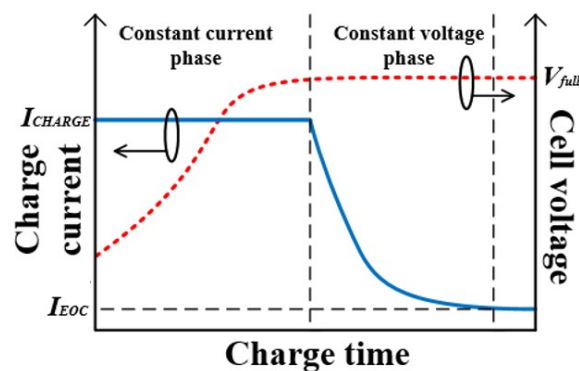


Figure 2. Constant Current-Constant Voltage charging algorithm.

The use of pulse charging has been shown to increase battery charge and energy efficiencies and to also reduce charge time [9,17,18]. It also has the added benefit of improved safety, since the relaxation times in between charge current pulses allows time for the  $\text{Li}^+$  to successfully intercalate and helps to prevent dendrite formation [14].

The challenge in the development and deployment of pulse charging algorithms is robustly finding and defining the conditions that produce the most efficient battery performance. Pulse charge currents have the different attributes, which can be at different levels and depending on the selection of these attributes and their levels, the battery output performance metrics, such as the battery charge and energy efficiencies, life cycle, and charge time, will differ. Pulse charging has been shown to have superior performances but the impact of these factors and their levels on the cycle life of the battery and its impedance parameters are seldom investigated. This paper seeks to address this shortcoming by using a design of experiments (DoE) approach, Taguchi orthogonal array (OA), and non-destructive techniques, such as electrochemical impedance spectroscopy, in order to determine the impact of pulse charge current factors and levels on battery cycle life and impedance parameters. This work also addresses the question of what factors have the most significant impact on the battery cycle life.

This paper is organized as follows: Section 2 provides a brief background on pulse charging and Taguchi OA. Section 3 reviews different techniques for evaluating the impact of charging parameters on battery characteristics. The design procedure is detailed in Section 4 and the experimental results are presented in Section 5. Conclusions are drawn in Section 6.

## 2. Background on Pulse Charging and Taguchi Orthogonal Array (OA)

### 2.1. Pulse Charging

Pulse charging involves using carefully selected and controlled charge current pulses to charge a battery. Figure 3a shows a macromodel of a pulse charger where by controlling the switch,  $S_w$ , charge current,  $I_c$ , is pulsed into the battery. Every pulse charge current that is applied to the battery has the following factors or attributes: peak current amplitude,  $I_{pk}$ , a duty cycle,  $D = t_{on}/T_p$ , and frequency,  $f$ , as shown in Figure 3b.

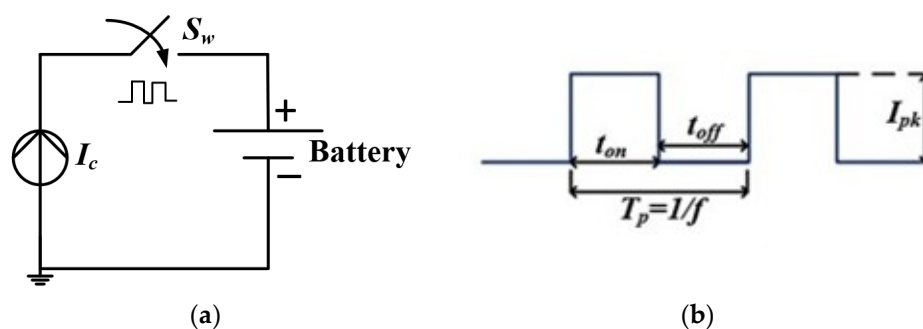


Figure 3. (a) Pulse charging micromodel; and (b) pulse waveform.

The selection of pulse attributes and their different levels also impacts the charge time, battery life cycle, and battery impedance parameters. The LiPo battery, which can be ideally modelled as a series resistance,  $R_s$ , which represents the resistance of the electrolyte and other contact resistances, in series with a parallel combination of the charge transfer resistance,  $R_{ct}$ , which represents the resistance of the kinetics of the Faradaic processes in the battery, and  $C_{dl}$ , which represents the charged areas between the electrode and electrolyte [19], is shown in Figure 4a. By using electrochemical impedance spectroscopy (EIS), the battery impedance parameters can be extracted from the Nyquist plot that is shown in Figure 4b. During pulse charging, the  $\text{Li}^+$  are able to intercalate properly in the anode, thereby reducing polarization voltage [20]. This, in turn, reduces energy losses in the battery, increasing the power transfer rate and improving charge and energy efficiencies. For a fixed pulse charge current

amplitude, lower duty cycles result in longer charge times, and higher duty cycles result in shorter charge times, but the battery is more susceptible to overcharging and overvoltage, two conditions that can be detrimental to the life cycle of the battery. For a fixed duty cycle, higher current amplitudes, resulting in higher average charge currents, will result in faster charge times, but the tendency of the battery to overcharge is high. The mathematical relation between  $I_{pk}$ ,  $D$ , and the average charge current  $I_{avg}$  can be expressed as:

$$I_{avg} = I_{pk} \cdot D \quad (1)$$

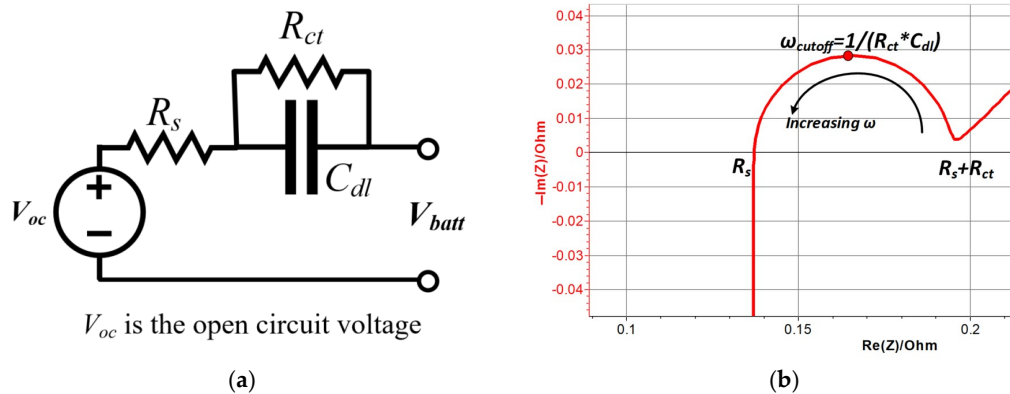


Figure 4. (a) LiPo battery equivalent circuit; and (b) Nyquist plot.

In terms of frequency, References [17,18] determined that pulsing at the frequency at which the battery impedance is minimum  $f_{zmin}$  resulted in faster charge times. These previous works determined the optimal pulse charge current factors that will result in a reduced charge time and increased battery charge and energy efficiencies. Short-term improvements in efficiencies and charge times have been recorded for pulse chargers [10,17,18,21], but it is important to determine how the pulse charge current attributes or factors affect the battery in the long term. This will impact the overall cost of a system, as if the proposed pulse charging algorithm reduces the life cycle of batteries or increases battery impedance parameter values, frequent replacements will be needed and that will impact the long-term cost of the battery-powered application. Other works, References [12,13] have investigated the impact of pulse charging on the life cycle of Li-ion batteries and found that pulse charging extended the life of Li-ion batteries when compared with dc charging protocols. These previous works, however, do not provide details regarding which factors of the pulse charge current have the most significant impact on the battery cycle life. By using a design of experiments approach, the impact of pulse charge current factors on battery cycle life and impedance parameters can be determined and evaluated.

## 2.2. Taguchi Orthogonal Arrays

A typical system undergoing an experiment is shown in Figure 5. Every experiment will have input factors, output responses, control factors, and uncontrollable factors. Input factors are variables that can be controlled to impact the output performance of a system. It is sometimes needed to determine how the output responses are impacted by the input, control factor levels, and uncontrollable factors. Designs of experiments are therefore methods that are used to acquire predictive information about systems. They can be used to optimize the output responses of a system by determining which input factors and their control factors impact the output responses the most. Taguchi OA are one of such methods that seeks to reduce the number of experiments without affecting the outcome of the system. Its design consists of balanced experimental sets where different input factors are at different levels. It can be used to evaluate the dependence of a certain output response on the input factor and input factor levels. It can also be designed to include uncontrollable factors, such as disturbances or



### 3. Techniques for Evaluation of Impact of Charging Parameters on Battery Characteristics

To determine the impact of charging factors on the cycle life and the impedance parameters of the battery, it is important to use techniques that give relevant information about the battery characteristics. These techniques can be classified as destructive and non-destructive [33].

#### 3.1. Destructive Techniques

Destructive techniques involve disassembling the battery to investigate the current state of its internal components, in terms of structure, chemical composition, and morphology. These techniques can be used to determine how different charging methods have impacted electrode morphology and structure [34,35], dendrite depositions [36,37], separator [38], and electrolyte degradation [39,40]. Investigation of these battery internal components can be performed while using scanning electron microscopy (SEM) [33–35,37,41], atomic force microscopy (AFM) [39,42], X-ray diffraction (XRD) [41,43–45], Raman microscopy [39,43], and electron probe microscopic analysis (EPMA) [46], of which SEM is the most popular.

#### 3.2. Non-Destructive Techniques

Non-destructive techniques do not involve the disassembling of the battery and have been known to be the popular ways for determining the battery impedance and performance across its life cycle. These techniques include cyclic voltammetry [44,46,47], impedance measurements, charge-discharge tests, and impedance spectroscopy [48], of which impedance spectroscopy is the most popular [49]. In this work, a combination of different non-destructive techniques will be used to characterize the battery aging, in effect its cycle life and the impact on battery impedance parameters.

By using the Taguchi OA design method that is described in Section 2 in combination with regression analysis, the factors and factor levels that have the greatest impact on the cycle life and impedance parameters of the battery can be determined. All of the results are compared with the benchmark CC-CV charging algorithm.

### 4. Design Procedure

Figure 6 shows the flow chart of the design procedure to determine the impact of pulse charge current factors on battery cycle life and impedance parameters. Before the Taguchi OA is designed and experiments conducted, the input factors and their levels, output responses, and uncontrollable factors should be defined. The number of factors and factor levels will indicate the size of the OA.

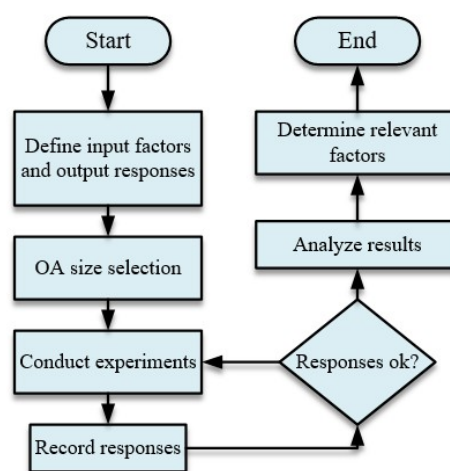


Figure 6. Design procedure for determining the impact of pulse current factors on LiPo battery.

*Input factors and output responses definition:* The input factors chosen are the duty cycle and frequency of the pulse charge current, and the ambient temperature at which the battery is charged at.

Three levels of duty cycle levels are chosen: 20%, 50%, and 80%. The impedance of the battery changes with frequency, as shown in Figure 7. At much lower frequencies, the impedance is much higher due to mass transport effects, and at high frequencies, the impedance is mainly due to the inductance of the battery, which is as a result of the electrodes [50]. Six levels of frequency are chosen to cover the frequency range of interest: 0.1 kHz, 1 kHz, 6 kHz,  $f_{zmin}$ , 50 kHz, and 100 kHz.  $f_{zmin}$  was included to investigate the impact it has on the battery characteristics. The ambient temperature chosen were 0 °C, 23 °C and 45 °C. The amplitude is not chosen as a factor so as to have a fair comparison with the CC-CV charging algorithm. Table 2 shows the input factors and their levels. The uncontrollable factors can be determined as the manufacturing variabilities on the batteries under test.

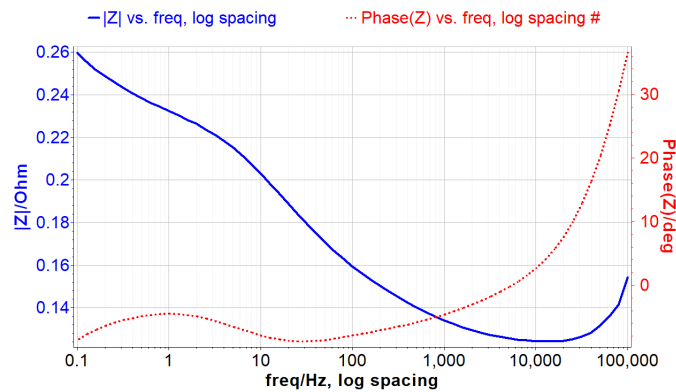


Figure 7. Bode magnitude and phase plot for equivalent battery circuit model.

Table 2. Control factors for Taguchi OA design.

Control factors	Factor levels					
	1	2	3	4	5	6
$D$	0.2	0.5	0.8	-	-	-
$T$ (°C)	0	23	45	-	-	-
$f$ (kHz)	0.1	1	6	$f_{zmin}$	50	100

The output responses are chosen to be battery cycle life,  $R_s$ , and  $R_{ct}$ .  $C_{dl}$  is not chosen as an output response since the magnitude of  $R_s$  and  $R_{ct}$  is much larger and will have more impact on the battery impedance, which can also impact the battery aging.

*OA size selection:* From Table 2, there are three control factors with two factors at three levels, and one factor at six levels. Hence, the OA to be designed has to be mixed level. An OA  $L_{36}(3^2 \times 6^1)$  was chosen. The design of this OA ensured that all input factors and their levels appeared an equal number of times. This OA is shown in Table 3.

**Table 3.** Taguchi orthogonal array.

Factors				Factors			
No.	T	D	f	No.	T	D	f
1	23	0.2	12k	19	0	0.8	12k
2	45	0.8	100	20	0	0.5	6k
3	45	0.2	50k	21	0	0.2	1k
4	45	0.2	6k	22	0	0.2	100
5	45	0.5	100k	23	23	0.2	100k
6	0	0.8	12k	24	0	0.5	6k
7	0	0.2	100	25	45	0.5	100k
8	45	0.8	1k	26	23	0.2	100k
9	23	0.5	1k	27	23	0.8	50k
10	0	0.2	1k	28	45	0.2	50k
11	0	0.5	50k	29	23	0.8	6k
12	45	0.5	12k	30	23	0.5	100
13	23	0.8	50k	31	0	0.5	50k
14	45	0.5	12k	32	0	0.8	100k
15	45	0.8	1k	33	45	0.2	6k
16	45	0.8	100	34	23	0.5	1k
17	23	0.5	100	35	23	0.8	6k
18	23	0.2	12k	36	0	0.8	100k

*Experiments and response analysis:* Experiments are conducted according to Table 3 and responses recorded and procedure is repeated until the battery ages significantly. At the end of the experiments, the responses are then analyzed while using the Taguchi S/N ratios, ANOM, and ANOVA. From these results, the factors that impact battery cycle life and impedance parameters can be determined. By decomposing the variance and computing the sum of squares, the effects of any of the factors can be determined from the sum of squares, which can be expressed as:

$$SS_{F_n} = \sum_{L_n} \left( n_{L_n} \cdot \left( \frac{1}{n_{L_n}} \sum_{i_{L_n}} O_{i_{L_n}j} - \bar{O} \right)^2 \right) \quad (3)$$

where  $O_j$  the output response,  $n_{L_n}$  is the number of output responses corresponding to level  $n$ , and  $i_{L_n}$  denotes the rows corresponding to level  $n$  responses only.

## 5. Experimental Results

Figure 8 shows the experimental test setup for running the experiments, according to Table 3. New 600 mAh 3.7 V LiPo batteries were first characterized at 0% SoC (state of charge) by using EIS to determine the battery impedance parameters. Battery impedance characteristics were measured by performing an EIS using a Versastat Potentiostat [51] and the Nyquist plots analyzed by using the Simplex method [52] for curve fitting to obtain battery impedance parameters. The  $f_{zmin}$  of the batteries was determined to be 12 kHz. Battery capacity measurements were also performed. The batteries were then placed in a temperature chamber, TestEquity model 107 [53], and experiments conducted according to Table 3. The batteries were subjected to a charge rate of 0.5C. After charging, when the batteries reached a state of charge (SoC) of 100%, the batteries were allowed to rest for one hour before being discharged at 0.5C until a SoC of 0% was attained. EIS measurements were then performed at this SoC. Both pulse and CC-CV charging algorithms used the same charge and discharge rate of 0.5C.

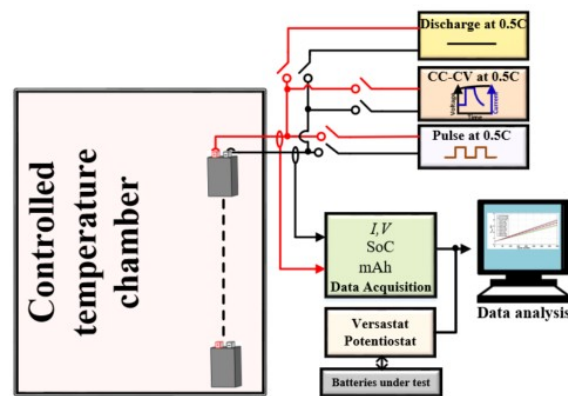


Figure 8. Experimental setup for determining impact of charge algorithms on battery.

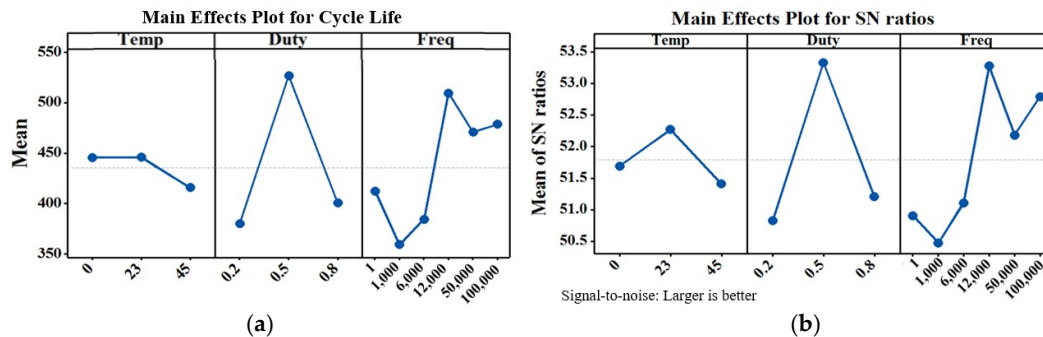
After about 400 cycles, the final EIS was performed and the battery impedance parameters extracted. All the EIS measurements were performed at 0% SoC. The battery cycle life was estimated from the recorded capacity measurements by using regression analysis and the cycle number at which the battery capacity is 80% of the original capacity recorded. The output responses are shown in Table 4.

Table 4. Output responses.

Factors				Factors			
No.	Cycle Life	$R_s$	$R_{ct}$	No.	Cycle Life	$R_s$	$R_{ct}$
1	583	0.8604	0.08091	19	873	0.9420	0.16680
2	370	0.8680	0.09468	20	308	0.9100	0.15500
3	239	0.9200	0.09845	21	438	0.9020	0.10390
4	421	0.9200	0.09845	22	360	0.9020	0.10390
5	763	0.8590	0.12000	23	295	0.8604	0.08091
6	446	0.9420	0.16680	24	214	0.9100	0.15500
7	213	0.9020	0.10390	25	755	0.8590	0.12000
8	258	0.8680	0.09468	26	250	0.8604	0.08091
9	545	0.8589	0.06816	27	486	0.9000	0.08174
10	303	0.9020	0.10390	28	408	0.9200	0.09845
11	512	0.9100	0.15500	29	377	0.9000	0.08174
12	388	0.8590	0.12000	30	828	0.8589	0.06816
13	309	0.9000	0.08174	31	871	0.9100	0.15500
14	311	0.8590	0.12000	32	401	0.9420	0.16680
15	215	0.8680	0.09468	33	593	0.9200	0.09845
16	268	0.8680	0.09468	34	396	0.8589	0.06816
17	434	0.8589	0.06816	35	393	0.9000	0.08174
18	456	0.8604	0.08091	36	408	0.9420	0.16680

Figure 9 shows the main effects plot and the S/N ratio, the larger-the-better, respectively, of the LiPo battery cycle life. It can be seen from Figure 9 that the duty cycle of the pulse charge current has a great impact on the battery cycle life and pulsing at 50% resulted in the longest cycle life. The temperature at which the battery is charged also had an impact on the cycle life, and from Figure 9, charging at 45 °C produced the shortest cycle life. Charging at  $f_{zmin}$  also impacts the battery, as it is at this frequency that the battery impedance is minimum, and hence less heating losses. Charging at 20% duty cycle produced the shortest cycle life due to the higher peak current used at this duty cycle to maintain the same average charge current, according to Equation (1). Higher peak currents can be detrimental to the battery life cycle. The factor levels that resulted in a longer battery cycle life were  $f = 12 \text{ kHz}$  ( $f_{zmin}$ ),  $D = 0.5$ , and  $T = 23 \text{ }^\circ\text{C}$ . By computing the ANOVA from the responses in Table 4, the ANOVA table can be obtained, as shown in Table 5. From this table, it is seen that duty cycle had

the largest impact on the cycle life, contributing 57.5%, as already determined from Figure 9. The next largest contribution was attributed to the frequency at which the pulse charge current operated, which contributed 39.8% to the total sum of squares.



**Figure 9.** (a) Main effects plot for battery cycle life; (b) Main effects plot of SN ratios for battery cycle life.

**Table 5.** Analysis of variance (ANOVA) table for output responses.

Cycle Life				
Factor	Degrees of Freedom	Sum of Squares	Mean Square	F
Duty Cycle	2	152,562	76,281	2.41
Frequency	5	105,460	21,092	0.58
Temperature	2	7221	3611	0.1
Total		265,243		
$R_s$				
Factor	Degrees of Freedom	Sum of Squares	Mean Square	F
Duty Cycle	2	0.004654	0.002327	3.02
Frequency	5	0.007104	0.001421	1.85
Temperature	2	0.013494	0.006747	13.41
Total		0.025252		
$R_{ct}$				
Factor	Degrees of Freedom	Sum of Squares	Mean Square	F
Duty Cycle	2	0.003193	0.001596	1.59
Frequency	5	0.007084	0.001417	1.45
Temperature	2	0.025525	0.012762	38.84
Total		0.035802		

Evaluating the impact of pulse charging parameters on the battery impedance parameters,  $R_s$ , and  $R_{ct}$ , the main effects plots and the S/N ratio, smaller the better, plots are shown in Figures 10 and 11. From the ANOVA table, the frequency at which the pulse charger operates had the second largest effect on the  $R_s$ , and  $R_{ct}$  values. The ambient temperature had the greatest impact on the impedance parameter values, contributing 53.4% and 71.3% to the total sum of squares for  $R_s$ , and  $R_{ct}$ , respectively. This is as expected, as temperature causes the accelerated aging of the battery [54]. The degradation in  $R_s$  and  $R_{ct}$  may be due to electrolyte decomposition, increase in surface film growth, reduction in active materials [44,46,49,55], and other effects that are produced due to various side chemical reactions that usually occur at the electrode/electrolyte interface [49]. These result in different degradations at the anode and cathode. Cathode degradation can arise from structural changes that occur during charge and discharge cycles while anode degradation can arise from increase in surface film growth (SEI) [54]. As a result of these degradations,  $R_s$  and  $R_{ct}$  increase as the battery ages, as shown in Figure 12.

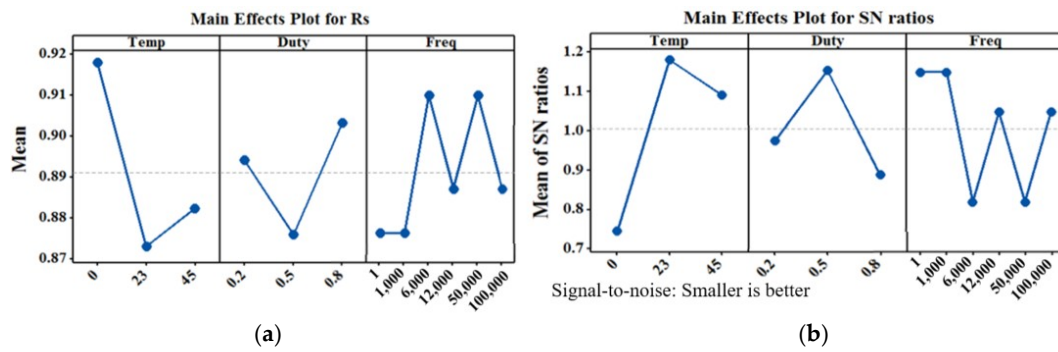


Figure 10. (a) Main effects plots for  $R_s$ ; (b) Main effects plots of SN for  $R_s$ .

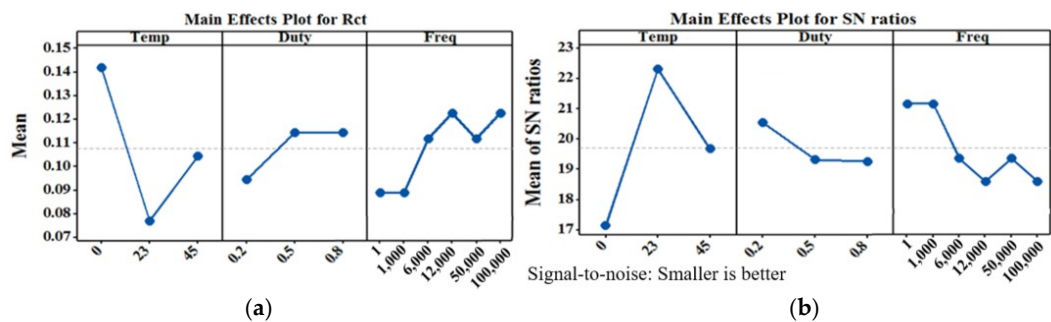


Figure 11. (a) Main effects plot for  $R_{ct}$ ; (b) Main effects plots of SN for  $R_{ct}$ .

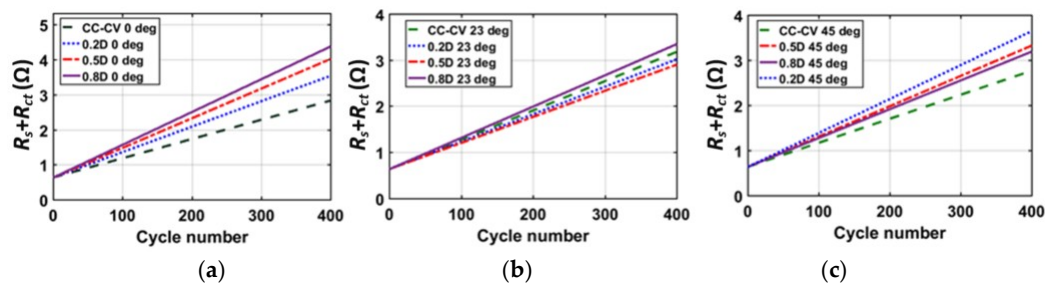


Figure 12. Trend of  $R_s$  and  $R_{ct}$  vs charge/discharge cycles, (a) at 0 °C; (b) at 23 °C; (c) at 45 °C.

From Figure 12, batteries that were subjected to pulse charging were compared with the benchmark CC-CV charging algorithm across different ambient temperatures. It can be seen that, at room temperature, the  $R_s + R_{ct}$  of the battery pulsed at 50% duty cycle was lower across the charge and discharge cycles when compared to the battery subjected to the CC-CV charging algorithm.

By using the accelerated aging effect [56], the cycle life of batteries subjected to pulsing at optimal values obtained from [18], i.e.,  $f = 12.6 \text{ kHz}$  ( $f_{Zmin}$ ) and  $D = 0.5$ , was compared to the benchmark CC-CV charging algorithm and plotted in Figure 13. It was observed that the pulse charged batteries attained more than 100 extra cycles when compared to the CC-CV charged batteries. This is due to the rest periods in the pulses that allows for the effective intercalation of the  $\text{Li}^+$  before the next application of the pulse, thereby preventing capacity fading due to the buildup of lithium deposits.

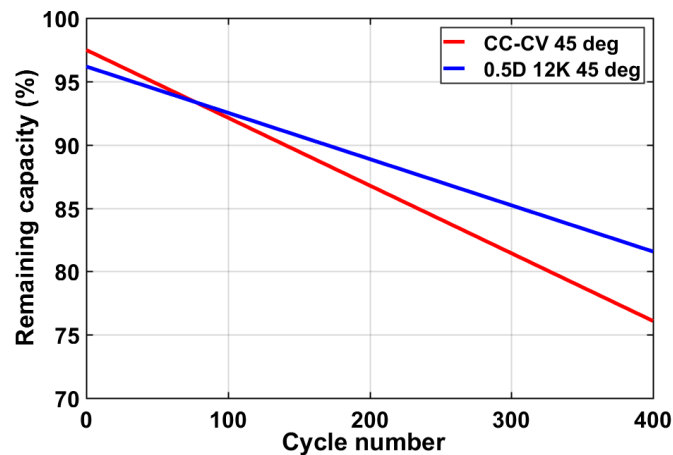


Figure 13. Cycle life comparison of CC-CV charged battery and pulse charged battery.

## 6. Conclusions

The influence of pulse charging parameters and ambient temperature at which the battery is charged on LiPo battery impedance parameters and life cycle has been determined. Battery impedance parameter values increased as the number of charge and discharge cycles increased. This is due to the various side chemical reactions that occur in the battery as it ages. The byproducts of these reactions impact the battery impedance. Batteries that were subjected to pulse charging at 50% duty cycle at room temperature had lower impedance values when compared to batteries subjected to CC-CV at the same temperature. Results from the accelerated aging of the battery indicated that pulse charging at the optimal values resulted in an increase of an additional 100 cycles when compared to the benchmark method CC-CV. In terms of determining which factor and factor levels of the pulse charge current affected the cycle life of the batteries, the Taguchi OA approach was used. It was deduced that the duty cycle of the pulse charge current played a major role in battery cycle life extension, followed by frequency at which the battery is charged. Ambient temperature impacted the battery impedance parameters greatly.

This work has demonstrated the impact of pulse charge current factors and factor levels on the cycle life of the battery. Accelerated life cycle tests have also proven that batteries subjected to the pulse charging at the optimal parameters can result in longer cycle life when compared to batteries that were subjected to the CC-CV charging algorithm.

**Author Contributions:** Conceptualization, J.M.A.-B. and A.G.-E.; Methodology, J.M.A.-B.; Software, J.M.A.-B.; Validation, J.M.A.-B.; Formal Analysis, J.M.A.-B.; Investigation, J.M.A.-B.; Resources, A.G.-E. and E.S.-S.; Writing-Original Draft Preparation, J.M.A.-B.; Writing-Review & Editing, J.M.A.-B., A.G.-E., and E.S.-S.; Supervision, A.G.-E. and E.S.-S.

**Funding:** This research received no external funding.

**Acknowledgments:** The authors want to acknowledge Ankita Bhat of the Center for Bioelectronics, Biosensors, and Biochips (C3B®) in the department of Biomedical Engineering at Texas A&M University, College Station, TX, USA, for support in performing battery impedance measurements.

**Conflicts of Interest:** The authors declare no conflict of interest.

## References

1. PR Newswire Association LLC, Lithium-Ion Battery Market is Expected to Reach \$46.21 Billion, Worldwide, by 2022. Available online: <https://www.prnewswire.com/news-releases/lithium-ion-battery-market-is-expected-to-reach-4621-billion-worldwide-by-2022-575386231.html> (accessed on 12 March 2018).
2. Global Market for Lithium-Ion Batteries—Forecast, Trends & Opportunities 2014–2020. Available online: <https://www.researchandmarkets.com/reports/2904215/global-market-for-lithium-ion-batteries> (accessed on 12 March 2018).
3. Grand View Research, Battery Market Size, Share | Industry Research Report, 2024. Available online: <https://www.grandviewresearch.com/industry-analysis/battery-marketvol> (accessed on 23 March 2018).
4. Reddy, T.B. *Linden's Handbook of Batteries*, 4th ed.; McGraw Hill Professional: New York, NY, USA, 2010.
5. Meyer, W.H. Polymer electrolytes for lithium-ion batteries. *Adv. Mater. (Deerfield Beach, Fla.)* **1998**, *10*, 439–448. [CrossRef]
6. Piqué, G.V.; Bergveld, H.J. State-of-the-Art of Integrated Switching Power Converters. In *Analog Circuit Design: Low Voltage Low Power; Short Range Wireless Front-Ends; Power Management and DC-DC*; Steyaert, M., Roermund, A.v., Baschiroto, A., Eds.; Springer Netherlands: Dordrecht, The Netherlands, 2012; pp. 259–281.
7. Iyengar, A.; Tripathi, A.; Basarur, A.; Roy, I. Unified Power Management Framework for Portable Media Devices. In Proceedings of the IEEE International Conference on Portable Information Devices, Orlando, FL, USA, 25–29 May 2007; pp. 1–5.
8. Lu, Y.H.; Simunic, T.; Micheli, G.d. Software controlled power management. Available online: [http://seelab.ucsd.edu/papers/ylu\\_codes99.pdf](http://seelab.ucsd.edu/papers/ylu_codes99.pdf) (accessed on 1 April 2018).
9. Yin, M.D.; Cho, J.; Park, D. Pulse-Based Fast Battery IoT Charger Using Dynamic Frequency and Duty Control Techniques Based on Multi-Sensing of Polarization Curve. *J. Energies* **2016**, *9*, 209. [CrossRef]
10. Chen, L.-R. A Design of an Optimal Battery Pulse Charge System by Frequency-Variation Technique. *IEEE TIE* **2007**, *54*, 398–405. [CrossRef]
11. Purushothaman, B.K.; Landau, U. Rapid Charging of Lithium-Ion Batteries Using Pulsed Currents. *JES* **2006**, *153*, A533. [CrossRef]
12. Popov, B.N.; Haran, B.S.; Durairajan, A.; White, R.; Podrazhansky, Y.; Cope, R.C. Studies on capacity fade of Li-ion cells cycled using pulse and DC charging protocols. In Proceedings of the Name of the 197th Electrochemical Society meeting, Toronto, ON, Canada, 14–18 May 2000.
13. Li, J.; Murphy, E.; Winnick, J.; Kohl, P.A. The effects of pulse charging on cycling characteristics of commercial lithium-ion batteries. *J. Power Sources* **2001**, *102*, 302–309. [CrossRef]
14. Ely, D.R.; García, R.E. Heterogeneous Nucleation and Growth of Lithium Electrodeposits on Negative Electrodes. *JES* **2013**, *160*, A668. [CrossRef]
15. Wang, Q.; Ping, P.; Zhao, X.; Chu, G.; Sun, J.; Chen, C. Thermal runaway caused fire and explosion of lithium ion battery. *J. Power Sources* **2012**, *208*, 210–224. [CrossRef]
16. Shen, W.; Vo, T.T.; Kapoor, A. Charging algorithms of lithium-ion batteries: An overview. In Proceedings of the 2012 7th IEEE Conference on Industrial Electronics and Applications (ICIEA), Singapore, Singapore, 18–20 July 2012; pp. 1567–1572.
17. Boadu, J.M.A.; Abouzied, M.; Sanchez-Sinencio, E. An Efficient and Fast Li-ion Battery Charging System Using Energy Harvesting or Conventional Sources. *IEEE TIE* **2018**, *65*, 7383–7394.
18. Boadu, J.M.A.; Guiseppi-Elie, A.; Sanchez-Sinencio, E. Search for Optimal Pulse Charging Parameters for Li-ion Polymer Batteries Using Taguchi Orthogonal Arrays. *IEEE TIE* **2018**, *65*, 8982–8992.
19. Randles, J.E.B. Kinetics of rapid electrode reactions. *Discuss. Faraday Soc.* **1947**, *1*, 11–19. [CrossRef]
20. Savoye, F.; Venet, P.; Millet, M.; Groot, J. Impact of Periodic Current Pulses on Li-Ion Battery Performance. *IEEE TIE* **2012**, *59*, 348–3488. [CrossRef]
21. Chen, L.-R. Design of Duty-Variation Voltage Pulse Charger for Improving Li-Ion Battery-Charging Response. *IEEE TIE* **2009**, *56*, 480–487.
22. Pundir, R.; Chary, G.H.V.C.; Dastidar, M.G. Application of Taguchi method for optimizing the process parameters for the removal of copper and nickel by growing *Aspergillus* sp. *Water Resour. Ind.* **2016**. [CrossRef]

23. Shahbazian, A.; Davood, A.; Dabirsiaghi, A. Application of Taguchi Method to Investigate the Effects of Process Factors on the Production of Industrial Piroxicam Polymorphs and Optimization of Dissolution Rate of Powder. *Iran. J. Pharm. Res. IJPR* **2016**, *15*, 395. [PubMed]
24. Pang, J.S.; Ansari, M.N.M.; Zaroog, O.S.; Ali, M.H.; Sapuan, S.M. Taguchi design optimization of machining parameters on the CNC end milling process of halloysite nanotube with aluminium reinforced epoxy matrix (HNT/Al/Ep) hybrid composite. *HBRC J.* **2014**, *10*, 138–144. [CrossRef]
25. Hsu, C.C.; Chien, C.S.; Wei, T.Y.; Li, Y.T.; Li, H.F. Taguchi DoE for ceramic substrate SMT defects improvement. In Proceedings of the 2016 11th International Microsystems, Packaging, Assembly and Circuits Technology Conference (IMPACT), Taipei, Taiwan, 26–28 October 2016; pp. 381–384.
26. Dudhe, R.; Ayyalusamy, S.; Desai, T. Optimization of BAW Resonator for Wireless Applications using Taguchi's Orthogonal Array Method. Available online: [https://www.researchgate.net/profile/Ravishankar\\_Dudhe2/publication/303719442\\_Optimization\\_of\\_BAW\\_Resonator\\_for\\_Wireless\\_Applications\\_using\\_Taguchi's\\_Orthogonal\\_Array\\_Method/links/574f1e0b08ae1880a820f7f4.pdf](https://www.researchgate.net/profile/Ravishankar_Dudhe2/publication/303719442_Optimization_of_BAW_Resonator_for_Wireless_Applications_using_Taguchi's_Orthogonal_Array_Method/links/574f1e0b08ae1880a820f7f4.pdf) (accessed on 23 January 2018).
27. Deo, R.; Likhite, A.A.; Zanwar, D.R.; Majumdar, G. Design of experiments by Taguchi method in agricultural research. *J. Soils Crop.* **2007**, *17*, 320–325.
28. Wang, S.C.; Chen, Y.L.; Liu, Y.H.; Huang, Y.S. A fast-charging pattern search for li-ion batteries with fuzzy-logic-based Taguchi method. In Proceedings of the 2015 IEEE 10th Conference on Industrial Electronics and Applications (ICIEA), Auckland, New Zealand, 15–17 June 2015; pp. 855–859.
29. Liu, Y.H.; Luo, Y.F. Search for an Optimal Rapid-Charging Pattern for Li-Ion Batteries Using the Taguchi Approach. *IEEE TIE* **2010**, *57*, 3963–3971. [CrossRef]
30. Wang, S.C.; Huang, J.W.; Liu, Y.H.; Hsieh, C.H. The implementation of consecutive orthogonal array method on searching optimal five step charging pattern for Lithium-ion batteries. In Proceedings of the 2011 9th World Congress on Intelligent Control and Automation, Taipei, Taiwan, 21–25 June 2011; pp. 358–363.
31. Phadke, M.S. *Quality Engineering Using Robust Design*, 1st ed.; Prentice Hall: Upper Saddle River, NJ, USA, 1989.
32. Taguchi, G. *Experimental Designs*; Maruzen Publishing Company: Tokyo, Japan, 1976.
33. Williard, N.; Sood, B.; Osterman, M.; Pecht, M. Disassembly methodology for conducting failure analysis on lithium-ion batteries. *J. Mater. Sci. Mater. Electron.* **2011**, *22*, 1616. [CrossRef]
34. Scipioni, R.; Jørgensen, P.S.; Ngo, D.; Simonsen, S.B.; Liu, Z.; Yakal-Kremski, K.J.; Wang, H.; Hjelm, J.; Norby, P.; Barnett, S.A.; Jensen, S.H. Electron microscopy investigations of changes in morphology and conductivity of LiFePO<sub>4</sub>/C electrodes. *J. Power Sources* **2016**, *307*, 259–269. [CrossRef]
35. Freitag, S.; Berger, C.; Gelb, J.; Weisenberger, T.B.C. Li-Ion Battery Components—Cathode, Anode, Binder, Separator—Imaged at Low Accelerating Voltages with ZEISS FE-SEMs, Zeiss White Paper, Carl Zeiss Microscopy GmbH. Available online: [https://p.widencdn.net/nih1gr/EN\\_wp\\_Battery\\_Low\\_Accelerating\\_Voltages\\_ZEISS-FE\\_SEMs](https://p.widencdn.net/nih1gr/EN_wp_Battery_Low_Accelerating_Voltages_ZEISS-FE_SEMs) (accessed on 23 March 2018).
36. Kong, L.; Xing, Y.; Pecht, M.G. In-Situ Observations of Lithium Dendrite Growth. *IEEE Access* **2018**, *6*, 8387–8393. [CrossRef]
37. Orsini, F.; Pasquier, A.D.; Beaudoin, B.; Tarascon, J.M.; Trentin, M.; Langenhuisen, N.; de Beer, E.; Notten, P. In situ Scanning Electron Microscopy (SEM) observation of interfaces within plastic lithium batteries. *J. Power Sources* **1998**, *76*, 19–29. [CrossRef]
38. Chan, J.Y.; Kim, J.H.; Seunghoon, N.; Park, C.R.; Yang, S.J. Rational Design of Nanostructured Functional Interlayer/Separator for Advanced Li-S Batteries. *Adv. Funct. Mater.* **2018**, 1707411. [CrossRef]
39. Jeong, S.; Inaba, M.; Iriyama, Y.; Abe, T.; Ogumi, Z. Surface film formation on a graphite negative electrode in lithium-ion batteries: AFM study on the effects of co-solvents in ethylene carbonate-based solutions. *Electrochimica Acta* **2002**, *47*, 1975–1982. [CrossRef]
40. Waag, W.; Käbitz, S.; Sauer, D.U. Experimental investigation of the lithium-ion battery impedance characteristic at various conditions and aging states and its influence on the application. *Appl. Energy* **2013**, *102*, 885–897. [CrossRef]
41. Aurbach, D.; Zinigrad, E.; Cohen, Y.; Teller, H. A short review of failure mechanisms of lithium metal and lithiated graphite anodes in liquid electrolyte solutions. *Solid State Ion.* **2002**, *148*, 405–416. [CrossRef]

42. Jeong, S.; Inaba, M.; Mogi, R.; Iriyama, Y.; Abe, T.; Ogumi, Z. Surface Film Formation on a Graphite Negative Electrode in Lithium-Ion Batteries: Atomic Force Microscopy Study on the Effects of Film-Forming Additives in Propylene Carbonate Solutions. *Langmuir* **2001**, *17*, 8281–8286. [CrossRef]
43. Shim, J.; KostECKI, R.; Richardson, T.; Song, X.; Striebel, K.A. Electrochemical analysis for cycle performance and capacity fading of a lithium-ion battery cycled at elevated temperature. *J. Power Sources* **2002**, *112*, 222–230. [CrossRef]
44. Ramadass, P.; Durairajan, A.; Haran, B.S.; White, R.E.; Popov, B.N. Capacity fade studies on spinel based Li-ion cells. In Proceedings of the Seventeenth Annual Battery Conference on Applications and Advances, Long Beach, CA, USA, 18 January 2002; pp. 25–30.
45. Itou, Y.; Ukyo, Y. Performance of LiNiCoO<sub>2</sub> materials for advanced lithium-ion batteries. *J. Power Sources* **2005**, *146*, 39–44. [CrossRef]
46. Zhang, D.; Haran, B.S.; Durairajan, A.; White, R.E.; Podrazhansky, Y.; Popov, B.N. Studies on capacity fade of lithium-ion batteries. *J. Power Sources* **2000**, *91*, 122–129. [CrossRef]
47. Lundgren, C.A.; Xu, K.; Jow, T.R.; Allen, J.; Zhang, S.S. *Springer Handbook of Electrochemical Energy*; Springer: Berlin Heidelberg, 2017; pp. 449–494. Available online: <https://www.springer.com/us/book/9783662466568> (accessed on 20 March 2018).
48. UTröltzsch; Kanoun, O.; Tränkler, H. Characterizing aging effects of lithium ion batteries by impedance spectroscopy. *Electrochimica Acta* **2006**, *51*, 1664–1672.
49. Vetter, J.; Novák, P.; Wagner, M.R.; Veit, C.; Möller, K.; Besenhard, J.O.; Winter, M.; Wohlfahrt-Mehrens, M.; Vogler, C.; Hammouche, A. Ageing mechanisms in lithium-ion batteries. *J. Power Sources* **2005**, *147*, 269–281. [CrossRef]
50. Jossen, A. Fundamentals of battery dynamics. *J. Power Sources* **2006**, *154*, 530–538. [CrossRef]
51. Ametek Scientific Instruments, VersaSTAT 4|Potentiostat Galvanostat|Princeton Applied Research. Available online: <https://www.ameteksi.com/products/potentiostats/single-channel/versastat-series/versastat-4> (accessed on 20 April 2018).
52. Dincer, I. *Comprehensive Energy Systems*. Elsevier, Posted February 21, 2018. Available online: <https://www.sciencedirect.com/referencework/9780128149256/comprehensive-energy-systems> (accessed on 2 March 2018).
53. TestEquity, TestEquity 107 Benchtop Temperature Chamber (Environmental Chamber). Available online: <https://www.testequity.com/products/1592/> (accessed on 20 April 2018).
54. Leng, F.; Tan, C.M.; Pecht, M. Effect of Temperature on the Aging rate of Li Ion Battery Operating above Room Temperature. *Sci. Rep.* **2015**, *5*, 12967. [CrossRef] [PubMed]
55. Ning, G.; Haran, B.; Popov, B.N. Capacity fade study of lithium-ion batteries cycled at high discharge rates. *J. Power Sources* **2003**, *117*, 160–169. [CrossRef]
56. Ecker, M.; Gerschler, J.B.; Vogel, J.; Käbitz, S.; Hust, F.; Dechent, P.; Sauer, D.U. Development of a lifetime prediction model for lithium-ion batteries based on extended accelerated aging test data. *J. Power Sources* **2012**, *215*, 248–257. [CrossRef]

